Effective destruction of perfluorooctanoic acid by zero-valent iron laden biochar obtained from carbothermal reduction: Experimental and simulation study

Min Yang [a], Xiaolei Zhang [a], Yicheng Yang [a], Qiang Liu [a*], Long D. Nghiem [b], Wenshan Guo [b], Huu Hao Ngo [b*]

[a] *School of Environmental and Chemical Engineering, Shanghai University, Shanghai 200444, China*

[b] *Centre for Technology in Water and Wastewater, School of Civil and Environmental Engineering, University of Technology Sydney, Sydney, NWS 2007, Australia*

*Corresponding authors:

Qiang Liu

School of Environmental and Chemical Engineering, Shanghai University, Shanghai 200444, China, Email: qliu@shu.edu.cn

Huu Hao Ngo

School of Civil and Environmental Engineering, University of Technology Sydney, Sydney, NWS 2007, Australia, HuuHao.Ngo@uts.edu.au

Abstract

This study investigated the degradation of perfluorooctanoic acid (PFOA) on zerovalent iron-laden biochar (BC-ZVI) prepared by carbothermal reduction. Results show that over 99% PFOA can be removed by BC-ZVI in hydrothermal conditions under 240 ℃ within 6 h. The maximum defluorination rate of 63.2% was achieved after 192 h, and this outcome was significantly better than biochar (BC) and zero-valent iron (ZVI) alone. The short-chain perfluorinated compounds (PFCs) and perfluoroheptanal were detected in the liquid phase after degradation, suggesting that the degradation of PFOAs by BC-ZVI followed the Kolbe decarboxylation process. XRD and SEM-EDS analyses strongly suggested that carbothermal reduction could avoid the agglomeration of ZVI loaded onto biochar, which helped make the PFOA degradation more efficient. The frontier molecular orbital theory calculated by density functional theory revealed there were two possibilities for ZVI loading on BC (edged or internal loading), while the edge loaded ZVI had a greater tendency to provide electrons for the defluorination of PFOA than internally loaded ZVI.

Keywords

PFOA, zero-valent iron-laden biochar, reductive defluorination, DFT calculation

Introduction

Per- and polyfluoroalkyl substances (PFASs) are persistent organic chemicals that are widely employed in antifouling coatings, surfactants, and fire-fighting foams (Kwok et al., 2013; Lindstrom et al., 2011; Prevedouros et al., 2006). Of these PFASs, perfluorooctanoic acid (PFOA) is the most common perfluorinated compound characterized by high thermal, chemical and biological stability owing to the abundance of recalcitrant fluoride-carbon bonds (Armitage et al., 2009; O'Hagan, 2008). As a new type of persistent organic pollutant, PFOA is found worldwide in multi-media environments, such as surface water (Zhang et al., 2016), soil (Chen et

al., 2017), groundwater (Houtz et al., 2013) and riverbed sediments (Loi et al., 2011). It has also been detected in human blood and breast milk due to the enrichment *via* food chain (Chimeddulam & Wu, 2013; He et al., 2015; Xu et al., 2014; Zhao et al., 2011). For these reasons, the U.S. Environmental Protection Agency (EPA) set a drinking water advisory on the combined level of PFOA and PFOS at 70 ng L^{-1} (EPA, 2016).

PFOA is resistant to most wastewater biological treatment processes (Zareitalabad et al., 2013) such as activated sludge (Guo et al., 2010) and membrane bioreactor (Yu et al., 2009). To date there are several physicochemical methods deemed to be valid for PFOA removal (Chularueangaksorn et al., 2013; Stasinakis et al., 2013; Tian et al., 2016; Trojanowicz et al., 2018; Trojanowicz et al., 2018; Wang et al., 2014; Zhuo et al., 2017). Of these, adsorption using engineered adsorbents such as biochar (Askeland et al., 2020), powdered activated carbon (Bo et al., 2016) and layered double hydroxides (Yun et al., 2020), membrane separation such as nanofiltration (Bao et al., 2019) and reverse osmosis filtration (Liu et al., 2012) have demonstrated significant PFOA removal efficacy. However, both adsorption and membrane separation will only transfer PFOA from one medium to another instead of completely detoxifying them. In order to alleviate the polluting effects of PFOA, oxidation treatment to completely mineralize or partially decompose the PFOA molecules has been the subject of many studies (Trojanowicz et al., 2018; Zhang et al., 2016). It was reported that advanced oxidation processes, such as Fenton reaction, could degrade PFOA into short chain perfluoroalkyl carboxylic acids (PFCAs) (Trojanowicz et al., 2018) *via* hydroxyl radical (·OH). Similarly, sulfate radical ($SO_4^{\cdot-}$) produced from persulfate ($S_2O_8^{2-}$) was also proven to be effective in PFOA degradation (Zhang et al., 2019).

In recent years, a lot of studies have reported that zero-valent metals (e.g., Fe^0 and Zn^0) are effective in the reductive defluorination of PFOA (Blotevogel et al., 2018). For example, Hori et al. (2006) found high temperature treatment could promote the degradation of PFOAs by zero-valent ion (ZVI), where the defluoridation efficiency reached 51%. Xia and Liu. (2020) indicated that the degradation of PFOA by ZVI nanoparticles could be accelerated by the irradiation of UVC light. Liu et al. (2020c) reported that the removal of PFOA could be increased by 20% when ZVI mixed with biochar. However, the application of ZVI in practice is limited by the high cost and difficulty in material preparation. To resolve these drawbacks, Lawrinenko et al. (2016) developed a novel method of pyrolyzing bio-renewable feedstocks and iron oxides to produce biochar-zero valent iron (BC-ZVI), where the prepared material exhibited both the physicochemical properties of ZVI and biochar. In contrast to ZVI prepared by borohydride reduction approach, BC-ZVI obtained from the co-pyrolysis of biomass with iron oxides is more environmentally friendly and economical because it does not require additional chemical reagents (Marrero-Alfonso et al., 2009). However, the application of the engineered materials on PFOA degradation and the accompanying mechanisms have not yet been well documented.

Recently, density functional theory (DFT) has been widely used to understand the complex mechanism which cannot be proven by experimental investigation, identify the degradation mechanism and reaction rate of pollutant removal (Chen et al., 2017; Niu et al., 2013; O'Hagan, 2008; Yuan et al., 2017). In their work, Zhang et al. (2019) combined DFT calculation with experiment to characterize the reaction process of $SO_4^{\cdot-}$ to degrade PFOA. Blotevogel et al. (2018) estimated the half-lives for the reductive PFOA defluorination step by Fe^0 and Zn^0 through DFT calculations. Bentel et al. (2020) calculated the degradation rate of different types of PFASs

through DFT, and proposed new designs for easily degradable PFASs. On the other hand, material structure and reaction performance could be evaluated by DFT analysis. Wu et al. (2017) analyzed the catalytic reduction ability of Pt/Pd nanoalloy for oxygen through frontier molecular orbital theory utilizing DFT calculation. It is expected that DFT theory can provide insightful information on the degradation of PFOA by BC-ZVI from the perspective of structural morphology, which could add critical information to the experimental results.

In this study, we prepared BC-ZVI through simultaneous pyrolysis of corn stover and ferric chloride, and used it to degrade PFOA. In order to study the mechanisms of BC-ZVI on PFOA degradation, the removal of PFOA, apparent defluoridation efficiency and degradation intermediates were assessed. The morphology and structural changes of BC-ZVI before and after the reaction were characterized. Moreover, DFT calculation served to optimize the structure of BC-ZVI clusters with different Fe loading status. Meanwhile, the effect of loading status on the degradation of PFOA was studied through frontier molecular orbital theory. This paper could provide useful information for the application of BC-ZVI to effectively treat PFOA.

2. Materials and Methods

Perfluorooctanoic acid (96%) and the standards of perfluoroheptanoic acid (PFHpA), perfluorohexanoic acid (PFHxA), perfluorovaleric acid (PFPeA), perfluorobutyric acid (PFBA), perfluoropropionic acid (PFPrA) and perfluoroacetic acid (TFA) were purchased from Shanghai Aladdin Biochemical Technology Co., China. Other commonly used chemical reagents such as ammonium acetate, methanol, ferric trichloride, sodium fluoride and zero-valent iron powder (marked with ZVI) were of analytical grade and obtained from Sinopharm Chemical Regent Co, China.

2.1 Biochar preparation

Corn straw was used for the preparation of biochar. The raw biomass was collected from Chongming Island, Shanghai, rinsed with tap water, ground and passed through a 0.15 mm sieve. To load Fe species onto sample, 10.0 g biomass and equivalent ferric chloride (10.0 g) were transferred into 200 mL deionized water, thoroughly mixed and oven dried at 105 ℃ for 48 h. Subsequently, the dried sample was evenly mixed with 10.0 g sieved raw biomass. The mixture was then loaded in a corundum boat, and heated with 5 ℃ min^{-1} in a temperature programmed furnace to 900 ℃ and remained for 2 h under 100 mL min^{-1} N_2 flow (99.99%). The obtained carbon was zero-valence iron loaded biochar (marked with BC-ZVI), and stored under N_2 for further use. Pristine biochar without Fe loading was also prepared (marked with BC) and subsequently included as a reference.

2.2 Degradation experiment

The degradation of PFOA was carried out in 50 mL stainless steel reaction kettle lined with a para-polyphenol (PPL) tube, where accommodating 20 mL PFOA solution (100 mg L^{-1}) and 1.0 g solid sample (BC, ZVI or BC-ZVI). The adsorption of PFOA by the PPL tube was found to be negligible (Figure S1). After N_2 purging (50 mL min^{-1}) for 15 min, the reactor was screwed up and heated in an oven at 10 ℃ min^{-1} to a predefined temperature (80-240 ℃) and kept for PFOA degradation. After the desired time (6-192 h), the reactor was quickly cooled down to room temperature by immersion into cold tap water. Afterward, 1 mL methanol was added to the liquid to quench the reaction. The solid sample was recovered by suction filtration, oven dried under 80 ℃ overnight and stored free from air. The filtrate was further filtrated with a 0.45 μm membrane (Aqueous, polyethersulfone PES), and a small aliquot was used to detect fluoride ion content immediately, while the rest was refrigerated under 4 ℃ for

the determination of PFOA and intermediates. All batch tests were carried out in triplicate and the control test free from solid sample was included.

Fluoride ion adsorption on solid sample was examined by batch test in the same reactor contained 20 mL sodium fluoride solution with a F^- content of 68.83 mg L^{-1} (the theoretical value of complete mineralization of 100 mg L^{-1} PFOA) and 1.0 g solid sample (BC, ZVI or BC-ZVI). F^- adsorption test was carried out in triplicate under the same condition as PFOA degradation. Control test free from solid sample (with sodium fluoride solution only) was also included. The dissolution of F- from the reactor (PPL tube) using 20 mL deionized water as background liquid was under the detection limit.

2.3 PFASs and F^- analysis

The concentration of PFOA and intermediates (C2-C8) in liquid were detected by an ultra-performance liquid chromatography (Agilent 7890 UHPLC) equipped with a triple quadrupole mass spectrometry (Agilent 6460 QQQ MSD) and Agilent Eclipse Plus C18 column (3.0 mm×100 mm, 3.5 μm). Prior to analysis, 50 μL 13C4-PFOA (MPFOA) (2 mg L^{-1}) was added to each sample and standard as an internal standard (IS). The recovery rate of final IS was 95%. Detailed procedure and the quality assurance and quality control procedures were provided in the Supporting Information.

The analysis of fluoride ion in liquid was carried out on an ion chromatography (IC) by conductivity detection (ICS-90, Dionex, Sunnyvale, CA) with a detection limit of 0.19 μg L^{-1}. The apparent defluoridation efficiency of PFOA was calculated by the following equation:

$$R = \frac{414C_{F^-}}{15 \times C_0 \times 19} \times 100\% \quad (1)$$

where R represents the apparent defluoridation efficiency of PFOA, %; C_{F^-} represents the concentration of F^- in solution, mg L^{-1}; C_0 denotes the initial concentration of PFOA in solution, mg L^{-1}; factor 15 corresponds to the number of fluorine atoms contained in one PFOA molecule, factor 19 is the atomic weight of fluorine, and factor 414 is the molecular weight of PFOA.

2.4 Solid phase characterization

X-ray diffraction (XRD) patterns of BC-ZVI and ZVI were obtained at 2θ of 5-90° with a D/max PBX ray diffraction (Rigaku Co.) using CuKα (k = 0.15406 nm) radiation operating with 40 mA and 40 k, and the test angle with a scan rate of 8 °/min were employed. X-ray photoelectron spectroscopic (XPS) analysis of fluorine element on sample was conducted using AlKα radiation on an X-ray photoelectron spectrometer (ESCALAB 220iXL, UK). Scanning electron microscopy coupled with energy dispersive X-ray analysis (SEM-EDS) was done on a FEI QUANTA FEG 250 scanning electron microscope using a 10 kV beam of about 1 nA. Images were collected using secondary electrons. Elemental maps were obtained by energy dispersive X-ray analysis using an Oxford Aztec EDS.

2.5 Computational modeling

Density functional theory (DFT) calculation was applied to optimize the molecular model and calculate the molecular frontier orbit through Gaussian 16 software by the B3LYP function in combination with 6-311++G (2d, 2p) basis set. The structure was optimized for the smallest amount of energy without using any symmetry constraints. Since biochar obtained under 900 ℃ usually contains marginal surface functional groups (Liu et al., 2020b), the defective graphene structure with unsaturated edge-carbon was constructed as a model of BC (Ding et al., 2020). The optimized structures of PFOA and BC-ZVI used in this work are illustrated in Table

S2.

3. Results and Discussion

3.1 Degradation of PFOA by BC-ZVI

Figure 1A displays the residue content of PFOA in liquid after 6 h of reaction with BC, ZVI, and BC-ZVI at 80-240 ℃. As observed, about 21%-33% PFOA was removed within 6 h under the control test free from adsorbent (BC) and reductant (ZVI), and the removal of PFOA seems to have little relevance to the reaction temperature. Similar phenomenon was also reported by Hao et al. (2021) and deemed to be related to the decomposition of less recalcitrant PFCAs. The limited PFOA removal from the control test suggested the sole hydrothermal treatment is ineffective for the degradation of this recalcitrant contaminant. BC alone received a better elimination performance of PFOA than the control test, and higher temperature was indeed favorable for the removal of PFOA. It was suggested that this is related to the active thermal motions of PFOA molecules under high temperature, which enhances the diffusion of PFOA and increases the contact between biochar (Ying et al., 2015). Similar to BC, the removal of PFOA by ZVI also presented a temperature-dependent pattern but much greater under 200-240 ℃, suggesting the removal of PFOA by ZVI could be significantly enhanced under high temperature, probably because the break of C-F bond is highly endothermic (Hori et al., 2006). One study reported that the iron oxides generated from the oxidization of Fe^0 have strong affinity to PFOA molecules, which may also contribute to the removal of this refractory contaminant (Zhang et al., 2018).

Among the materials investigated in this experiment, BC-ZVI revealed the best efficiency in removing PFOA. Notably, about 60%-70% PFOA was removed by

BC-ZVI under low temperature, and a maximum removal over 99% was achieved at 240 ℃. This is probably due to the high temperature provides abundant energy for the cleavage of C-F bond when reacting with BC-ZVI (Blotevogel et al., 2018). Inyang and Dickenson. (2017) reported that pinewood biochar could achieve a maximum removal efficiency of 94% for PFOA. As well, only 20% of input PFOA was removed by ZVI, and as BC was mixed to ZVI, the PFOA removal efficiency rose to 60% (Liu et al., 2020c). About results are less than the removal efficiency obtained by BC-ZVI in this study, demonstrating it is a promising material for the removal of PFOA. In a previous study (Wu et al., 2019), it was reported that a slight higher temperature (250 ℃) could achieved a PFOA degradation efficiency more than 99% within 30 min without any amendment. This result verified that reaction temperature is a critical factor affecting the removal efficiency of PFOA (Bentel et al., 2019), and more effort should be paid to develop efficient PFOA degradation methods to reduce energy input.

Fluoride content in liquid phase was monitored to identify the degree of PFOA destruction during the reaction. As observed from Figure 1B, the produced F^- ions in the control test were fairly low and depended scarcely on reaction temperature. The result of the test with BC was similar even though a slightly higher F^- content was detected. This suggests that only limited PFOA could be destroyed under hydrothermal conditions no matter the presence of biochar, which agrees well with PFOA removal results from Figure 1A. For ZVI tests, insignificant amounts of fluoride ions were generated after the reactions under low temperatures, while F^- concentration rose slightly with increasing temperature. This outcome verified that the thermo-induced reaction can promote the degradation of PFOA by ZVI alone as reported by Hori et al. (2006). However, the amount of F^- ions generated from the

reductive defluorination of PFOA by ZVI was still at a low level even at 240 ℃, which is inconsistent with the prominent removal of PFOA achieved by ZVI as indicated in Figure 1A. It was tentatively inferred that iron oxides resulting from the corrosion of ZVI during the reactions could adsorb the degradation products of PFOAs or fluoride ions (Liu et al., 2020c; Zhang et al., 2018).

From Figure 1B, it is evident that the fluorides generated from the test using BC-ZVI at 80-120 ℃ were almost identical to the test of BC, suggesting that the removal of PFOA by BC-ZVI at low temperature is dominated by adsorption. Although the loading of ZVI will reduce the specific surface area of biochar (Dong et al., 2017a), ZVI can serve as an active site for chemical adsorption to adsorb PFOA at low temperatures (Parenky et al., 2020). With increasing temperature, however, the amounts of fluoride increased, which coincides with the decay of PFOA under the presence of BC-ZVI. As a whole, the produced F^- ions by BC-ZVI after 6 h of reaction with PFOA (1.65 mg L^{-1}) accounted for only 2.4% of fluorides from the complete mineralization of 100 mg L^{-1} PFOA (68.83 mg L^{-1}), which reveals a large gap between PFOA removal. Therefore, the tests of F^- adsorption on BC, ZVI and BC-ZVI were carried out. The result (Figure S2) indicated about 9.1%, 4.3%, and 7.8% of F^- could be adsorbed within 6 h by BC, ZVI, and BC-ZVI, respectively. F-adsorption by biochar and ZVI was also reported by other researchers (Liu et al., 2020c), and which brings difficulty for the accurate evaluation of the extent of PFOA degradation. However, based on the limited sorption capacity of F^- ions, we strongly believed that the removal of PFOA by BC-ZVI is dominated by adsorption within limited reaction time (6 h).

Figure 1

To illustrate the dynamics, the removal of PFOA by BC-ZVI, ZVI and BC were further investigated under a prolonged period (24 h) under 240 ℃. As shown in Figure 2A, PFOA removal by BC-ZVI, ZVI and BC achieved equilibrium at about 6, 8 and 12 h, respectively. Both BC-ZVI and ZVI could achieve the maximum removal of PFOA (about 100 mg g^{-1}) despite the latter requiring a little longer reaction time, probably because BC-ZVI has more adsorptive sites than ZVI resulting from the special surface structure of biochar (Dong et al., 2017b; Petala et al., 2013; Zhu et al., 2009). For BC, a maximum PFOA removal capacity of 80.12 mg g^{-1} was reached at 12 h.

The pseudo-first-order and pseudo-second-order models were used to fit the kinetics of PFOA removal. As shown in Table 1, the decay of PFOA on BC-ZVI and ZVI followed the pseudo-second-order kinetics (R^2 = 0.999 and 0.997, respectively), suggesting the dominance of multi-molecular layer chemisorption in the removal of PFOA. The rate constant (K_2) followed the order of BC-ZVI (0.011) > ZVI (0.004), indicating the removal of PFOA by BC-ZVI was much faster in contrast to ZVI. The removal of PFOA by BC coincided more likely with the pseudo-first-order kinetics (R^2 = 0.998), revealing the privilege of monolayer physical adsorption of PFOA onto biochar surface. The fitting rate constant (K_1) of the adsorption of PFOA by biochar was 0.303, while the equilibrium adsorption amount (Q_e) reached 82.1 mg g^{-1}.

The intermediates during the reaction between BC-ZVI and PFOA at 240 ℃ were monitored to make clear the degradation route of PFOA. As observed from Figure 2B, a series of short-chain PFASs, such as PFHpA (C7), PFHxA (C6), PFPeA (C5), PFBA (C4), PFPrA (C3) and TFA (C2) were consecutively detected along with time, suggesting the degradation of PFOA is a typical stepwise defluorination process as previously reported (Bentel et al., 2020). It should be noted that perfluoroheptanal

($C_6F_{13}COF$) was also detected at the first 144 h of reaction, further demonstrating that the degradation of PFOA followed the Kolbe decarboxylation process (see section 3.2). The total decomposition products reached maximum (92% of the input PFOA) at 48 h, suggesting that PFOA were almost completely decomposed within this period. After 192 h, only 16.4% decomposition products remained in liquid, highlighting that a fairly high degree of complete mineralization can be achieved by BC-ZVI. Moreover, the concentration of TFA did not decline as expected, which meant that further decomposition of TFA was inhibited. According to Bentel et al. (2020), the bond energy of C-F at α-position of TFA is much larger than other short-chain PFASs, which required more energy to be decomposed.

Figure 2

Apparent defluoridation efficiency of PFOA on BC-ZVI was examined along with reaction (Figure S3). The ultimate apparent defluoridation efficiency was 63.2% and most identifiable fluorinated by-products were decomposed after 192 h. Figure 2B and the supplementary data suggest that not all fluorinated degradation by-products have been accounted for. Possible examples may include perfluorohexanal and perfluorovaleraldehyde (Wang et al., 2021). This finding suggested that most of PFOA could be completely broken down after 192 h of reaction using BC-ZVI. Zhang et al. (2019) reported that the advanced oxidation process involving sulfate radicals can remove 98.9% of PFOA at 144 h, and only 7.5% of short-chain PFCAs (relative to the initial PFOA) remain at 288 h. Lawal and Choi. (2018) noted that the maximum removal efficiency of PFOA by palladium-doped nanoscale ZVI was 92%, which was more closely associated with adsorption than defluorination. Compared with the PFOA degradation methods that have been investigated, the degradation of PFOA by BC-ZVI could achieve superior

removal efficiency and defluoridation efficiency without adding any other chemical reagents.

3.2 Solid-phase analysis

To elucidate the fate of fluorine, XPS analysis of BC-ZVI after the reaction at 80 ℃ and 240 ℃ was conducted and the detailed scans of F1s spectra are shown in Figure 3. After 6 h reaction with PFOA at 80 ℃, a strong characteristic peak around 689 eV was found on BC-ZVI (Figure 3A), which can be assigned to fluorine bonded carbon (Hori et al., 2006). This suggested PFOA or incompletely mineralized products were absorbed by BC-ZVI, further confirming the removal of PFOA by BC-ZVI under low temperature was mainly associated with physical adsorption. In contrast, BC-ZVI after the reaction with PFOA at 240 ℃ showed no peak corresponding to the species for fluorine around 678-698 eV (Figure 3B). As stated previously, PFOA was not detected at 240 ℃ and large amounts of fluoride ions were detected in the liquid phase, so it can be inferred that PFOA had already been decomposed by BC-ZVI. It can therefore be reasonably speculated that PFOA might be first adsorbed by BC-ZVI, and then decomposed by ZVI deposited on biochar to make the cleavage of carbon-fluoride bond under high temperature.

Figure 3

XRD pattern reveals a number of characteristic peaks (at 2θ of 44.77°, 65.17° and 82.53°) indexed to ZVI (Lawrinenko et al., 2016) can be found on BC-ZVI before reaction (Figure 4A), suggesting Fe^0 was successfully loaded on BC. However, these peaks weakened markedly after reaction with PFOA at 240 ℃. Conversely, the characteristic peaks of magnetite strengthened greatly. The development of iron mineral phases should be ascribed to the generation of iron oxides after ZVI oxidization during the reaction. It is consistent with other research, which showed that

ZVI loaded on biochar is still redox active (Oh et al., 2016). In addition, during the oxidation of ZVI, it can provide electrons to PFOA, thereby promoting its degradation (Liu et al., 2020c). At the same time, the formation of magnetite will reduce the contact between ZVI and PFOA, thus limiting the removal of PFOA (Zhang et al., 2018).

In contrast to BC-ZVI, the XRD spectra of ZVI (Figure 4B) suggest that part of ZVI was oxidized to magnetite and hematite after the reaction. In spite of this, the characteristic peaks of ZVI still remained stubbornly on the spectrum, which indicated that ZVI was no fully consumed during reaction. A possible explanation is that the aggregation of ZVI greatly diminished the interfaces between Fe^0 and liquid phase. After the oxidization of surface Fe^0, the internal ZVI was wrapped by the newly developed hematite, which further prevented the contact between ZVI and PFOA (Ruiz-Torres et al., 2018). The redox inert hematite is incapable of providing electrons, which could also inhibit the decomposition of PFOA (Phenrat et al., 2007). However, Zhang et al. (2018) demonstrated that hematite could facilitate the effective adsorption of PFOA. Therefore, these results suggested that hematite formation could inhibit ZVI contact with PFOA molecules and enhance the adsorption of PFOA on the biochar.

Figure 4

In addition, the dispersion of ZVI on biochar could inhibit ZVI agglomeration (Phenrat et al., 2007), where the even dispersion of ZVI could increase the proportion of surface Fe atoms and thus increase the number of surface active sites (Crane & Scott, 2012). On the other hand, bare ZVI was more easily oxidized during the reaction, which could inhibit the reactivity of ZVI with PFOA (Ruiz-Torres et al., 2018). For this reason, it could be assumed that ZVI loaded onto biochar was

uniformly dispersed on the biochar surface, where full contact between the PFOA molecules and ZVI was achieved.

To verify our hypothesis, SEM-EDS analysis of BC-ZVI was carried out. SEM image (Figure 5A) revealed that the surface of BC-ZVI had a layered and porous structure, which could provide abundant sites to facilitate PFOA adsorption. EDS mapping results (Figure 5B) suggested that Fe^0 distributed uniformly on the BC surface, where the aggregation of ZVI was inhibited. It was reported that ZVI could appear as a type of spherical core shell-like structure on the biochar surface, and be uniformly dispersed in the multi-level voids or surface of the material (Liu et al., 2020a). Thus, the formation of chain-like aggregates of ZVI was inhibited (Phenrat et al., 2007). This could make possible the contact between ZVI and PFOA on the biochar surface and further promote the complete degradation of PFOA.

Figure 5

On the basis of experimental results, the mechanism about the degradation of PFOA on BC-ZVI can be summarized as follows. First, PFOA is removed by BC-ZVI from the aqueous solution by adsorption. Subsequently, ZVI denotes electrons to promote the formation of perfluorooctanoic acid free radical ($C_7F_{15}COO\cdot$) from PFOA. Then, it goes through the Kolbe decarboxylation process to form perfluoroheptyl radicals ($C_7F_{15}\cdot$), and reacts with water to form $C_7F_{15}OH$. Finally, after conducting hydrolysis and defluorination twice, $C_6F_{13}COO^-$ is created. This process repeats until PFOA is completely mineralized, as indicated in Figure 6.

Figure 6

3.3 Molecular orbital analysis

The effect of different structures of BC-ZVI on the degradation of PFOA was studied. The elemental iron and its two loading statuses on biochar were used for

molecular orbital analysis by DFT calculation.

The frontier molecular orbital theory suggested that the interaction of the lowest unoccupied molecular orbital (LUMO) and the highest occupied molecular orbital (HOMO) of two molecules determined their possibilities to react, and the band gap energy (ΔE) between LUMO and HOMO can be used to describe the strength of the interaction. Figure 7 illustrates two things: firstly, the LUMO of PFOA and the HOMO of elemental iron; and secondly, the different combination of BC-ZVI clusters (internal load and edge load). The ΔE of PFOA and elemental iron were fairly low, indicating the interaction between Fe^0 and PFOA is significant, where ZVI could feasibly provide electrons for the degradation of PFOA. Compared with the internal load, edge-loaded BC-ZVI exhibits a lower ΔE, meaning that ZVI loaded on the edge of biochar was more active for interaction with PFOA, while the internally loaded ZVI tends to react with the PFOA adsorbed on biochar. Referring to quantum chemistry analysis of magnetite and hematite (Nagarajan & Chandiramouli, 2016; Rajeevgandhi et al., 2020), the ΔE between them and PFOA was 5.113 and 5.169, respectively, which are greater than the ΔE of the edge-loaded biochar and PFOA. This suggested that the interaction between oxidized ZVI and PFOA will be greatly reduced, which is consistent with the conclusions derived from this study.

Figure 7

Conclusion

This work explored the performance of Fe^0 loaded biochar on the degradation of PFOA. It was discovered that BC-ZVI prepared from carbothermal reduction could effectively inhibit the agglomeration of ZVI on biochar surface. The removal of PFOA increased significantly with the reaction temperature, where the maximum removal reached 99% within 6 h. Near complete degradation of PFOA could be

achieved after 192 h of reaction. According to the analysis, the degradation of PFOA with BC-ZVI was confirmed and the [-CF_2] units were gradually removed from the carbon chains through the Kolbe decarboxylation process with electrons provided by ZVI oxidation. The frontier molecular orbital theory showed the HUMO of PFOA and the LOMO of BC-ZVI using DFT calculation, suggesting different combination forms of BC and ZVI could have different degradation abilities for PFOA. Finally, the edge-loaded ZVI was found to have a greater tendency to interact with PFOA.

Acknowledgment

The authors acknowledge greatly the helps from Jinglin You (State Key Laboratory, Shanghai University) and Guosheng Shi (School of Environmental and Chemical Engineering, Shanghai University) on molecular orbital analysis. We also greatly appreciate the financial support from National Natural Science Foundation of China (No. 41877123) and the help from the Instrumental Analysis & Research Center of Shanghai University for sample characterization. The authors are also grateful to the research collaboration between Shanghai University and University of Technology Sydney.

Declaration of competing interest

The authors declare that they have no known competing financial interests or personal relationships that could have appeared to influence the work reported in this paper.

References

Armitage, J.M., MacLeod, M., Cousins, I.T. 2009. Response to Comment on "Comparative Assessment of the Global Fate and Transport Pathways of Long-Chain Perfluorocarboxylic Acids (PFCAs) and Perfluorocarboxylates (PFCs) Emitted from Direct Sources". *Environmental Science & Technology*, **43**(18), 7153-7154.

Askeland, M., Clarke, B.O., Cheema, S.A., Mendez, A., Paz-Ferreiro, J. 2020. Biochar sorption of PFOS, PFOA, PFHxS and PFHxA in two soils with contrasting texture. *Chemosphere*, **249**, 126072.

Bao, Y., Cagnetta, G., Huang, J., Yu, G. 2019. Degradation of Hexafluoropropylene Oxide Oligomer Acids as PFOA Alternatives in Simulated Nanofiltration Concentrate: effect of molecular structure. *Chemical Engineering Journal*, **382**, 122866.

Bentel, M.J., Yu, Y., Xu, L., Kwon, H., Li, Z., Wong, B.M., Men, Y., Liu, J. 2020. Degradation of Perfluoroalkyl Ether Carboxylic Acids with Hydrated Electrons: Structure-Reactivity Relationships and Environmental Implications. *Environ Sci Technol*, **54**(4), 2489-2499.

Bentel, M.J., Yu, Y., Xu, L., Li, Z., Wong, B.M., Men, Y., Liu, J. 2019. Defluorination of Per- and Polyfluoroalkyl Substances (PFASs) with Hydrated Electrons: Structural Dependence and Implications to PFAS Remediation and Management. *Environ Sci Technol*, **53**(7), 3718-3728.

Blotevogel, J., Giraud, R.J., Borch, T. 2018. Reductive defluorination of perfluorooctanoic acid by zero-valent iron and zinc: A DFT-based kinetic model. *Chemical Engineering Journal*, **335**, 248-254.

Bo, S., Ma, J., Sedlak, D.L. 2016. Chemisorption of Perfluorooctanoic Acid on Powdered Activated Carbon Initiated by Persulfate in Aqueous Solution. *Environmental Science & Technology*, **50**(14), 7618.

Chen, P., Zhang, L., Xue, Z.L., Wu, Y.D., Zhang, X. 2017. Density Functional Theory Study of the Reaction between d(0) Tungsten Alkylidyne Complexes and H2O: Addition versus Hydrolysis. *Inorg Chem*, **56**(12), 7111-7119.

Chimeddulam, D., Wu, K.Y. 2013. River water contaminated with perfluorinated compounds potentially posing the greatest risk to young children. *Chemosphere*, **90**(5), 1617-24.

Chularueangaksorn, P., Tanaka, S., Fujii, S., Kunacheva, C. 2013. Adsorption of perfluorooctanoic acid (PFOA) onto anion exchange resin, non-ion exchange resin, and granular-activated carbon by batch and column. *Desalination and Water Treatment*, **52**(34-36), 6542-6548.

Crane, R.A., Scott, T.B. 2012. Nanoscale zero-valent iron: future prospects for an emerging water treatment technology. *J Hazard Mater*, **211-212**, 112-25.

Ding, D., Yang, S., Qian, X., Chen, L., Cai, T. 2020. Nitrogen-doping positively whilst sulfur-doping negatively affect the catalytic activity of biochar for the degradation of organic contaminant. *Applied Catalysis B: Environmental*, **263**, 118348.

Dong, H., Deng, J., Xie, Y., Zhang, C., Jiang, Z., Cheng, Y., Hou, K., Zeng, G. 2017a. Stabilization of nanoscale zero-valent iron (nZVI) with modified biochar for Cr(VI) removal from aqueous solution. *J Hazard Mater*, **332**, 79-86.

Dong, H., Zhang, C., Hou, K., Cheng, Y., Deng, J., Jiang, Z., Tang, L., Zeng, G. 2017b. Removal of trichloroethylene by biochar supported nanoscale zero-valent iron in aqueous solution. *Separation and Purification Technology*, **188**, 188-196.

EPA, US. 2016. Drinking Water Health Advisories for PFOA and PFOS https://www.epa.gov/ground-water-and-drinking-water/drinking-water-health-advisories-pfoa-and-pfos.

Guo, R., Sim, W.J., Lee, E.S., Lee, J.H., Oh, J.E. 2010. Evaluation of the fate of perfluoroalkyl compounds in wastewater treatment plants. *Water Research*, **44**(11), 3476-3486.

Hao, S., Choi, Y.J., Wu, B., Higgins, C.P., Deeb, R., Strathmann, T.J. 2021. Hydrothermal Alkaline Treatment for Destruction of Per- and Polyfluoroalkyl Substances in Aqueous Film-Forming Foam. *Environ Sci Technol*, **55**(5), 3283-3295.

He, X., Dai, K., Li, A., Chen, H. 2015. Occurrence and assessment of perfluorinated compounds in fish from the Danjiangkou reservoir and Hanjiang river in China. *Food Chem*, **174**, 180-7.

Hori, H., Nagaoka, Y., Yamamoto, A., Sano, T., Yamashita, N., Taniyasu, S., Kutsuna, S., Osaka, I., Arakawa, R. 2006. Efficient decomposition of environmentally persistent perfluorooctanesulfonate and related fluorochemicals using zerovalent iron in subcritical water. *Environmental Science & Technology*, **40**(3), 1049-1054.

Houtz, E.F., Higgins, C.P., Field, J.A., Sedlak, D.L. 2013. Persistence of perfluoroalkyl acid precursors in AFFF-impacted groundwater and soil. *Environ Sci Technol*, **47**(15), 8187-95.

Inyang, M., Dickenson, E.R.V. 2017. The use of carbon adsorbents for the removal of perfluoroalkyl acids from potable reuse systems. *Chemosphere*, **184**, 168-175.

Kwok, K.Y., Yamazaki, E., Yamashita, N., Taniyasu, S., Murphy, M.B., Horii, Y., Petrick, G., Kallerborn, R., Kannan, K., Murano, K., Lam, P.K.S. 2013. Transport of Perfluoroalkyl substances (PFAS) from an arctic glacier to downstream locations: Implications for sources. *Science of the Total Environment*, **447**, 46-55.

Lawal, W.A., Choi, H. 2018. Feasibility Study on the Removal of Perfluorooctanoic Acid by Using Palladium-Doped Nanoscale Zerovalent Iron. *Journal of Environmental Engineering*, **144**(11), 04018115.

Lawrinenko, M., Laird, D.A., van Leeuwen, J.H. 2016. Sustainable Pyrolytic Production of Zerovalent Iron. *ACS Sustainable Chemistry & Engineering*, **5**(1), 767-773.

Lindstrom, A.B., Strynar, M.J., Libelo, E.L. 2011. Polyfluorinated Compounds: Past, Present, and Future. *Environmental Science & Technology*, **45**(19), 7954-7961.

Liu, C.S., Higgins, C.P., Wang, F., Shih, K. 2012. Effect of temperature on oxidative transformation of perfluorooctanoic acid (PFOA) by persulfate activation in water. *Separation & Purification Technology*, **91**, 46-51.

Liu, J., Jiang, J., Meng, Y., Aihemaiti, A., Xu, Y., Xiang, H., Gao, Y., Chen, X. 2020a. Preparation, environmental application and prospect of biochar-supported metal nanoparticles: A review. *Journal of Hazardous Materials*, **388**, 122026.

Liu, Q., Bai, X., Su, X., Huang, B., Wang, B., Zhang, X., Ruan, X., Cao, W., Xu, Y., Qian, G. 2020b. The promotion effect of biochar on electrochemical degradation of nitrobenzene. *Journal of Cleaner Production*, **244**, 118890.

Liu, Y., Ptacek, C.J., Baldwin, R.J., Cooper, J.M., Blowes, D.W. 2020c. Application of zero-valent iron coupled with biochar for removal of perfluoroalkyl carboxylic and sulfonic acids from water under ambient environmental conditions. *Sci Total Environ*, **719**, 137372.

Loi, E.I., Yeung, L.W., Taniyasu, S., Lam, P.K., Kannan, K., Yamashita, N. 2011. Trophic magnification of poly- and perfluorinated compounds in a subtropical food web. *Environ Sci Technol*, **45**(13), 5506-13.

Marrero-Alfonso, E.Y., Beaird, A.M., Davis, T.A., Matthews, M.A. 2009. Hydrogen Generation from Chemical Hydrides. *Industrial & Engineering Chemistry Research*, **48**(8), 3703-3712.

Nagarajan, V., Chandiramouli, R. 2016. DFT Studies on Interaction of H2S Gas with α-Fe2O3 Nanostructures. *Journal of Inorganic and Organometallic Polymers and Materials*, **26**(2), 394-404.

Niu, J., Lin, H., Gong, C., Sun, X. 2013. Theoretical and experimental insights into the electrochemical mineralization mechanism of perfluorooctanoic acid. *Environ Sci Technol*, **47**(24), 14341-9.

O'Hagan, D. 2008. Understanding organofluorine chemistry. An introduction to the C-F bond. *Chemical Society Reviews*, **37**(2), 308-319.

Oh, S.Y., Seo, Y.D., Ryu, K.S. 2016. Reductive removal of 2,4-dinitrotoluene and 2,4-dichlorophenol with zero-valent iron-included biochar. *Bioresour Technol*, **216**, 1014-21.

Parenky, A.C., Souza, N., Asgari, P., Jeon, J., Choi, H. 2020. Removal of Perfluorooctanesulfonic Acid in Water by Combining Zerovalent Iron Particles with Common Oxidants. *Environmental Engineering Science*, **37**(7), 472-481.

Petala, E., Dimos, K., Douvalis, A., Bakas, T., Tucek, J., Zboril, R., Karakassides, M.A. 2013. Nanoscale zero-valent iron supported on mesoporous silica: characterization and reactivity for Cr(VI) removal from aqueous solution. *J Hazard Mater*, **261**, 295-306.

Phenrat, T., Saleh, N., Sirk, K., Tilton, R.D., Lowry, G.V. 2007. Aggregation and sedimentation of aqueous nanoscale zerovalent iron dispersions. *Environmental Science & Technology*, **41**(1), 284-290.

Prevedouros, K., Cousins, I.T., Buck, R.C., Korzeniowski, S.H. 2006. Sources, fate and transport of perfluorocarboxylates. *Environmental Science & Technology*, **40**(1), 32-44.

Rajeevgandhi, C., Bharanidharan, S., Savithiri, S., Guganathan, L., Sugumar, P., Sathiyamurthy, K., Mohan, K. 2020. Synthesis, characterizations and quantum chemical calculations of the spinel structure of Fe3O4 nanoparticles. *Journal of Materials Science: Materials in Electronics*, **31**(23), 21419-21430.

Ruiz-Torres, C.A., Araujo-Martínez, R.F., Martínez-Castañón, G.A., Morales-Sánchez, J.E., Guajardo-Pacheco, J.M., González-Hernández, J., Lee, T.-J., Shin, H.-S., Hwang, Y., Ruiz, F. 2018. Preparation of air stable nanoscale zero valent iron functionalized by ethylene glycol without inert condition. *Chemical Engineering Journal*, **336**, 112-122.

Stasinakis, A.S., Thomaidis, N.S., Arvaniti, O.S., Asimakopoulos, A.G., Samaras, V.G., Ajibola, A., Mamais, D., Lekkas, T.D. 2013. Contribution of primary and secondary treatment on the removal of benzothiazoles, benzotriazoles, endocrine disruptors, pharmaceuticals and perfluorinated compounds in a sewage treatment plant. *Sci Total Environ*, **463-464**, 1067-75.

Tian, H., Gao, J., Li, H., Boyd, S.A., Gu, C. 2016. Complete Defluorination of Perfluorinated Compounds by Hydrated Electrons Generated from 3-Indole-acetic-acid in Organomodified Montmorillonite. *Sci Rep*, **6**, 32949.

Trojanowicz, M., Bartosiewicz, I., Bojanowska-Czajka, A., Kulisa, K., Szreder, T., Bobrowski, K., Nichipor, H., Garcia-Reyes, J.F., Nałęcz-Jawecki, G., Męczyńska-Wielgosz, S., Kisała, J. 2019. Application of ionizing radiation in decomposition of perfluorooctanoate (PFOA) in waters. *Chemical Engineering Journal*, **357**, 698-714.

Trojanowicz, M., Bojanowska-Czajka, A., Bartosiewicz, I., Kulisa, K. 2018. Advanced Oxidation/Reduction Processes treatment for aqueous perfluorooctanoate (PFOA) and

perfluorooctanesulfonate (PFOS) – A review of recent advances. *Chemical Engineering Journal*, **336**, 170-199.

Wang, F., Lu, X., Shih, K.M., Wang, P., Li, X. 2014. Removal of perfluoroalkyl sulfonates (PFAS) from aqueous solution using permanently confined micelle arrays (PCMAs). *Separation and Purification Technology*, **138**, 7-12.

Wang, J., Cao, C., Zhang, Y., Zhang, Y., Zhu, L. 2021. Underneath mechanisms into the super effective degradation of PFOA by BiOF nanosheets with tunable oxygen vacancies on exposed (101) facets. *Applied Catalysis B: Environmental*, **286**, 119911.

Wu, B., Hao, S., Choi, Y., Higgins, C.P., Deeb, R., Strathmann, T.J. 2019. Rapid Destruction and Defluorination of Perfluorooctanesulfonate by Alkaline Hydrothermal Reaction. *Environmental Science & Technology Letters*, **6**(10), 630-636.

Wu, J., Shan, S., Cronk, H., Chang, F., Kareem, H., Zhao, Y., Luo, J., Petkov, V., Zhong, C.-J. 2017. Understanding Composition-Dependent Synergy of PtPd Alloy Nanoparticles in Electrocatalytic Oxygen Reduction Reaction. *The Journal of Physical Chemistry C*, **121**(26), 14128-14136.

Xia, C., Liu, J. 2020. Degradation of perfluorooctanoic acid by zero-valent iron nanoparticles under ultraviolet light. *Journal of Nanoparticle Research*, **22**(7), 188.

Xu, J., Guo, C.S., Zhang, Y., Meng, W. 2014. Bioaccumulation and trophic transfer of perfluorinated compounds in a eutrophic freshwater food web. *Environ Pollut*, **184**, 254-61.

Ying, B., Lin, G., Jin, L., Zhao, Y., Wang, J. 2015. Effect of corn cob biochar on the adsorption of 2,4-Dichlorophenoxyacetic acid in soil. *Acta Scientiae Circumstantiae*, **35**(5), 1491-1497.

Yu, J., Hu, J., Tanaka, S., Fujii, S. 2009. Perfluorooctane sulfonate (PFOS) and perfluorooctanoic acid (PFOA) in sewage treatment plants. *Water Research*, **43**(9), 2399-2408.

Yuan, H., Xiao, P., Zheng, Y., Zhang, Q. 2017. DFT studies on the mechanism of Ag2 CO3 -catalyzed hydroazidation of unactivated terminal alkynes with TMS-N3 : An insight into the silver(I) activation mode. *J Comput Chem*, **38**(27), 2289-2297.

Yun, C., Ag, D., Wzab, C., Bdk, D., Jya, C., Ns, D., Jing, L., Mg, E., Mca, C. 2020. Mechanistic insights into fast adsorption of perfluoroalkyl substances on carbonate-layered double hydroxides. *Journal of Hazardous Materials*, **408**, 124815.

Zareitalabad, P., Siemens, J., Hamer, M., Amelung, W. 2013. Perfluorooctanoic acid (PFOA) and perfluorooctanesulfonic acid (PFOS) in surface waters, sediments, soils and wastewater – A review on concentrations and distribution coefficients. *Chemosphere*, **91**(6), 725-732.

Zhang, C., Tang, J., Peng, C., Jin, M. 2016. Degradation of perfluorinated compounds in wastewater treatment plant effluents by electrochemical oxidation with Nano-ZnO coated electrodes. *Journal of Molecular Liquids*, **221**, 1145-1150.

Zhang, Y., Moores, A., Liu, J., Ghoshal, S. 2019. New Insights into the Degradation Mechanism of Perfluorooctanoic Acid by Persulfate from Density Functional Theory and Experimental Data. *Environ Sci Technol*, **53**(15), 8672-8681.

Zhang, Y., Zhi, Y., Liu, J., Ghoshal, S. 2018. Sorption of Perfluoroalkyl Acids to Fresh and Aged Nanoscale Zerovalent Iron Particles. *Environ Sci Technol*, **52**(11), 6300-6308.

Zhao, Y.G., Wan, H.T., Law, A.Y., Wei, X., Huang, Y.Q., Giesy, J.P., Wong, M.H., Wong, C.K. 2011. Risk assessment for human consumption of perfluorinated compound-contaminated freshwater and marine fish from Hong Kong and Xiamen. *Chemosphere*, **85**(2), 277-83.

Zhu, H., Jia, Y., Wu, X., Wang, H. 2009. Removal of arsenic from water by supported nano zero-valent iron on activated carbon. *J Hazard Mater*, **172**(2-3), 1591-6.

Zhuo, Q., Xiang, Q., Yi, H., Zhang, Z., Yang, B., Cui, K., Bing, X., Xu, Z., Liang, X., Guo, Q., Yang, R. 2017. Electrochemical oxidation of PFOA in aqueous solution using highly hydrophobic modified PbO 2 electrodes. *Journal of Electroanalytical Chemistry*, **801**, 235-243.

Figures

Figure 1 (A) PFOA removal and (B) fluoride ion production by BC, ZVI and BC-ZVI within 6 h (100 mg L^{-1} of PFOA with 1.0 g sample)

Figure 2 (A) The amount of PFOA removed by BC, ZVI and BC-ZVI (100 mg L^{-1} of PFOA with 1.0 g sample) along with reaction under 240 ℃; (B) Profiles of by-product of PFOA degradation during the reaction with BC-ZVI at 240 ℃

Figure 3 XPS spectra of BC-ZVI after reaction with PFOA at (A) 80 ℃ and (B) 240 ℃

Figure 4 XRD patterns of (A) BC-ZVI and (B) ZVI before and after reaction with PFOA

Figure 5 SEM image of (A) BC-ZVI and (B) Fe elemental spot mapping of BC-ZVI measured by SEM-EDS

Figure 6 The mechanism of PFOA degradation by BC-ZVI (Kobel decarboxylation process)

Figure 7 Frontier molecular orbitals, and the energy of LUMO of PFOA and HOMO of elemental iron and different combination forms of BC-ZVI clusters

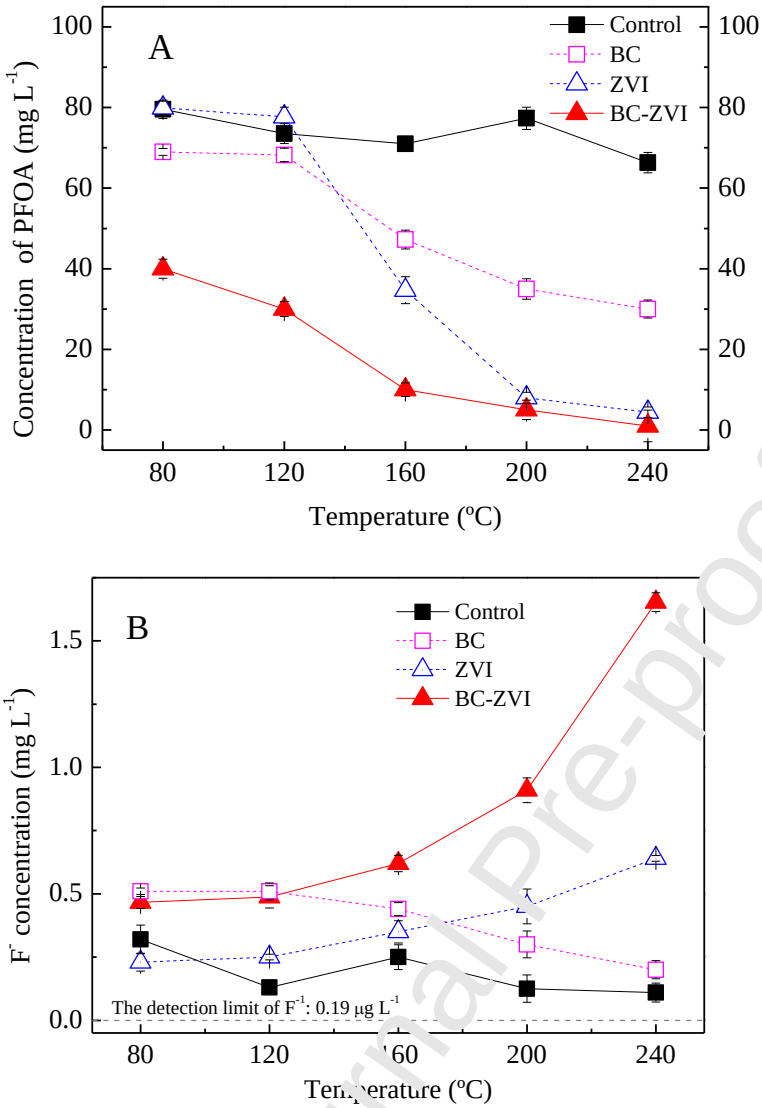

Figure 1 (A) PFOA removal and (B) fluoride ion production by BC, ZVI and BC-ZVI within 6 h (100 mg L^{-1} of PFOA with 1.0 g sample)

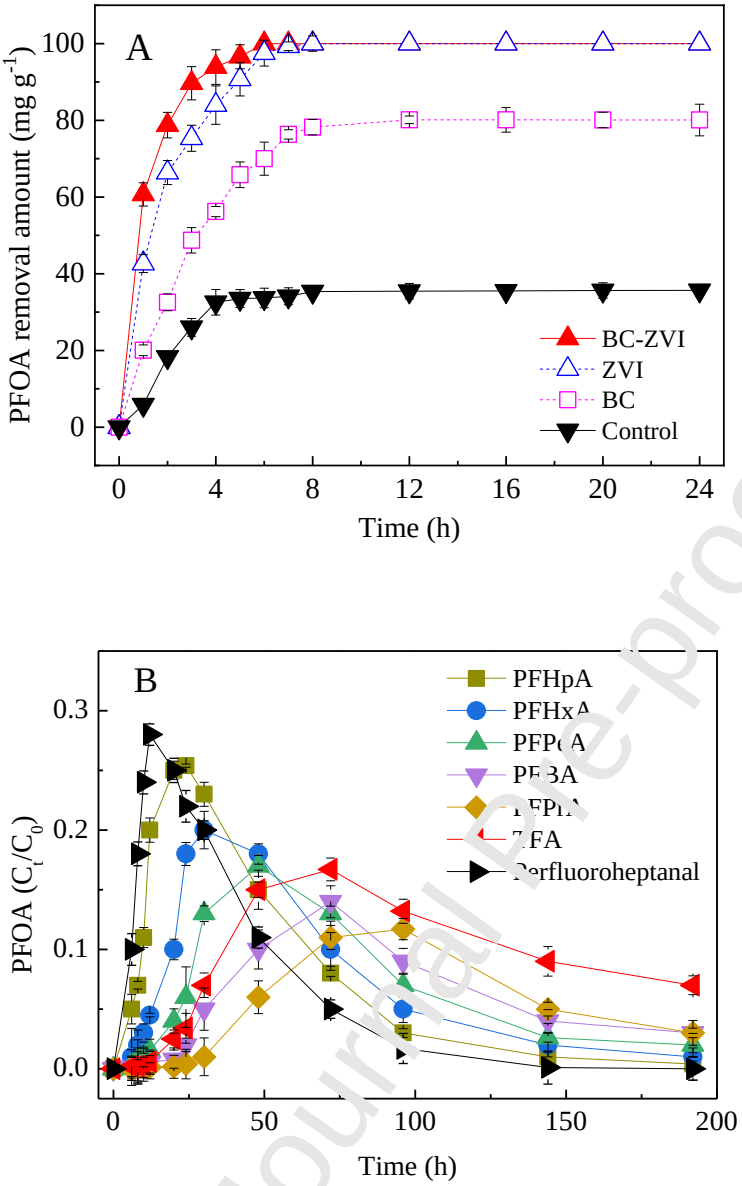

Figure 2 (A) The amount of PFOA removed by BC, ZVI and BC-ZVI (100 mg L^{-1} of PFOA with 1.0 g sample) along with reaction under 240 ℃; (B) Profiles of by-product of PFOA degradation during the reaction with BC-ZVI at 240 ℃

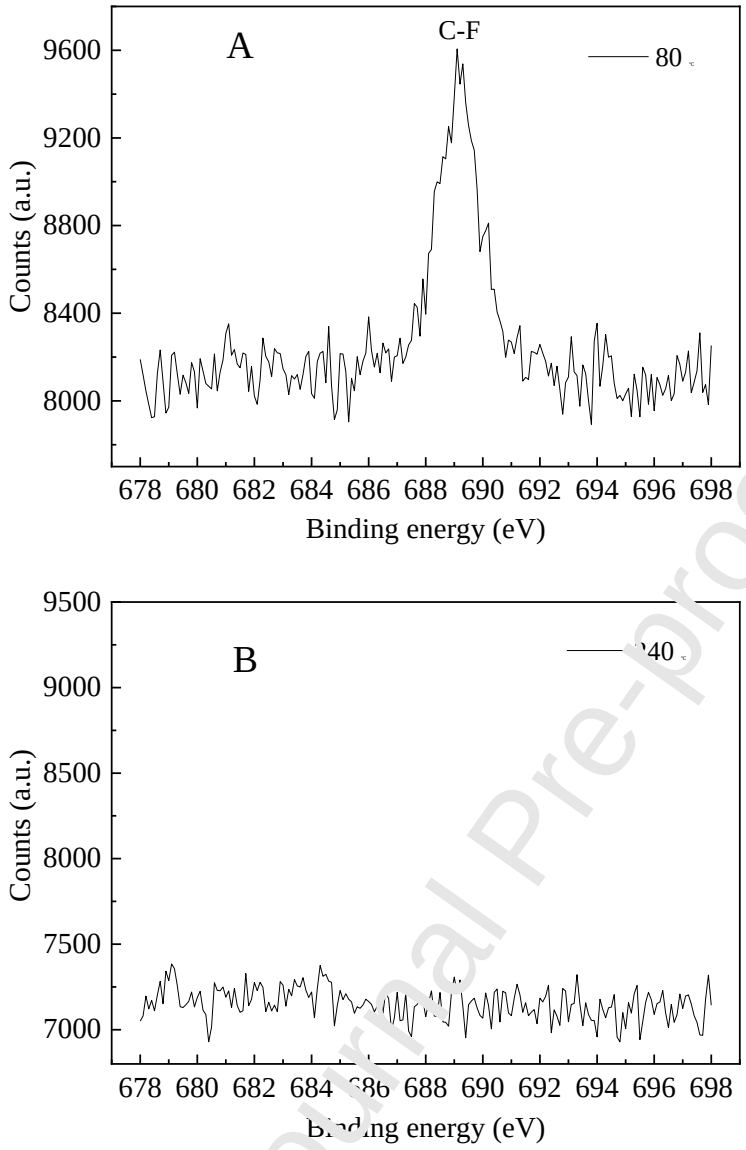

Figure 3 XPS spectra of BC-ZVI after reaction with PFOA at (A) 80 ℃and (B) 240 ℃

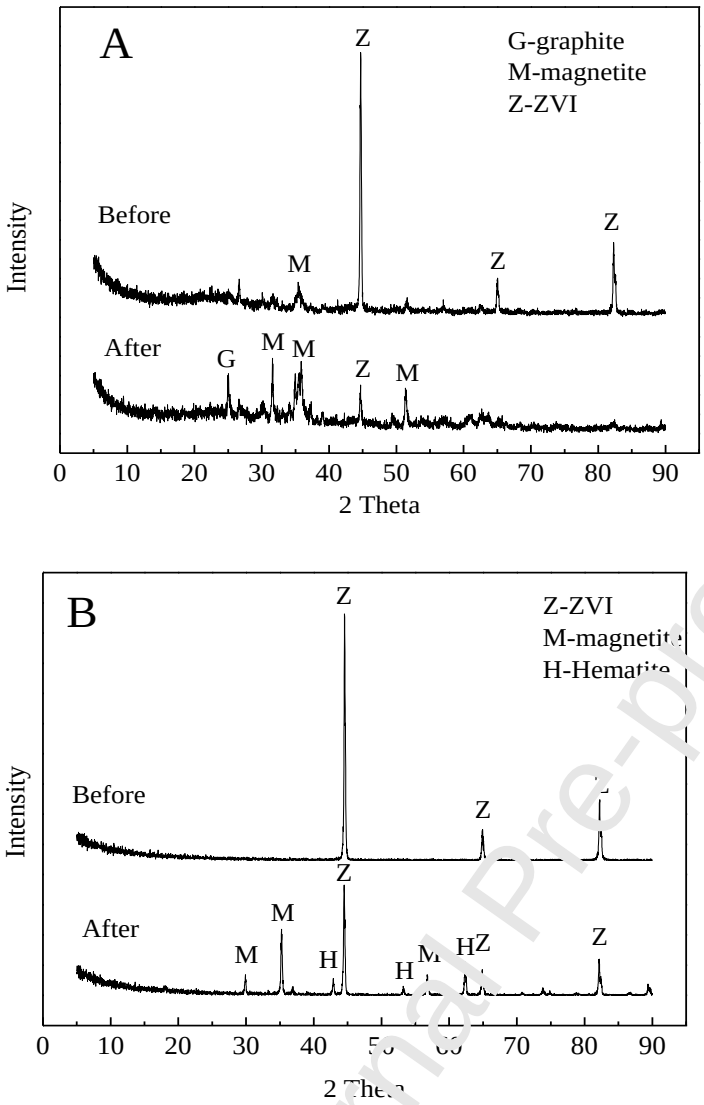

Figure 4 XRD patterns of (A) EG-ZVI and (B) ZVI before and after reaction with PFOA

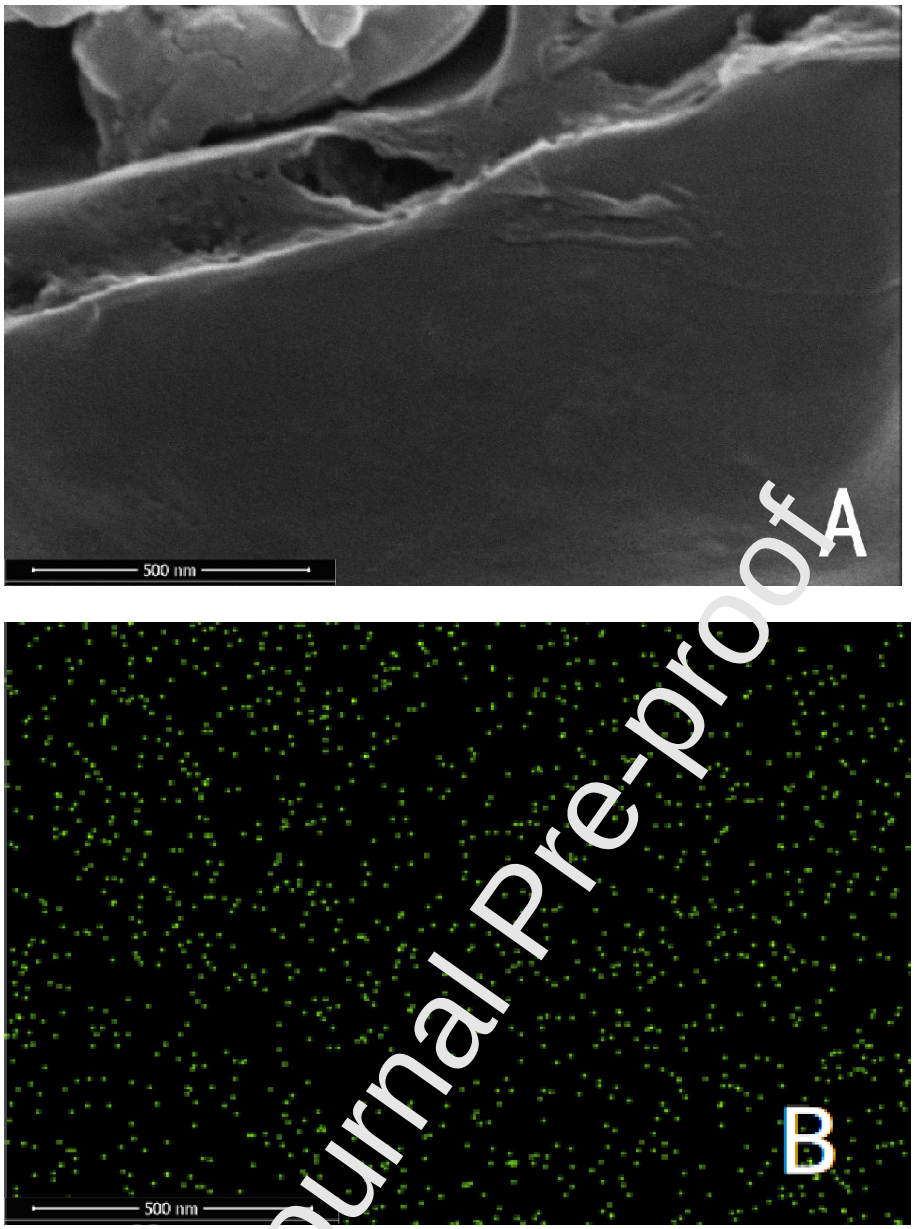

Figure 5 SEM image of (A) BC-ZVI and (B) Fe elemental spot mapping of BC-ZVI measured by SEM-EDS

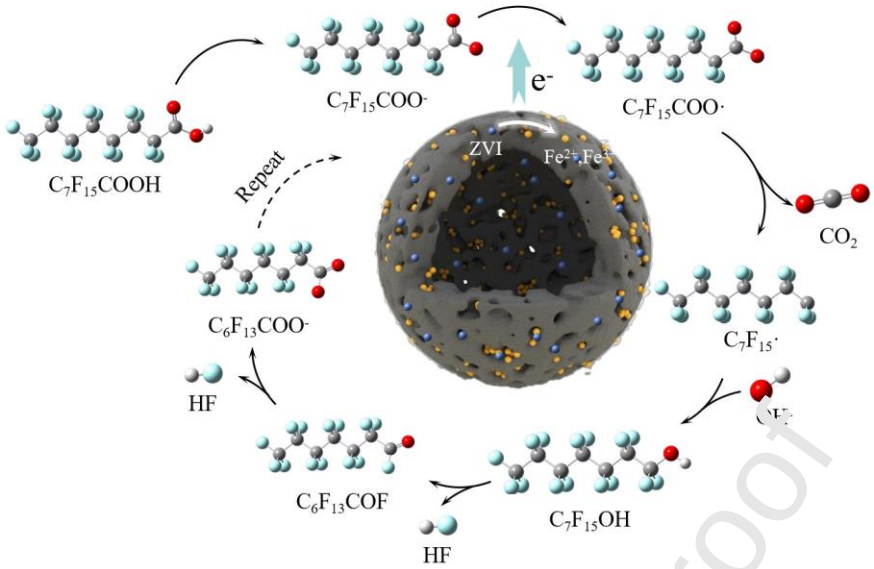

Figure 6 The mechanism of PFOA degradation by BC-ZVI (Kolbel decarboxylation process)

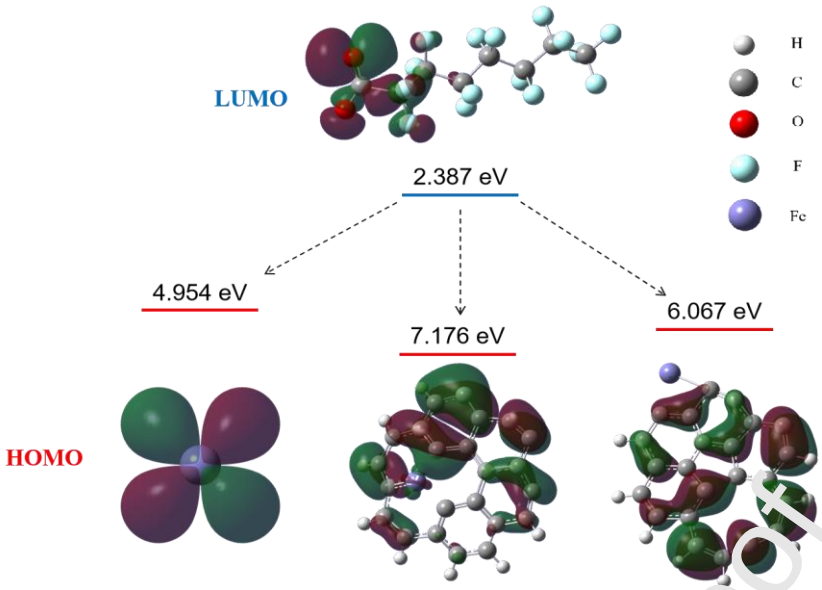

Figure 7 Frontier molecular orbitals, and the energy of LUMO of PFOA and HOMO of elemental iron and different combination forms of BC-ZVI cluster

Table

Table 1 Kinetic parameters of pseudo-first-order and pseudo-second-order models for PFOA removal by BC-ZVI, ZVI and BC

	Pseudo-first-order model			Pseudo-second-order model		
	Q_e	K_1	R^2	Q_e	K_2	R^2
BC-ZVI	98.8	0.045	0.996	112.5	0.011	0.999
ZVI	101.0	0.032	0.994	125.9	0.004	0.997
BC	82.1	0.303	0.991	96.2	0.004	0.962